Research Square

Preprints are preliminary reports that have not undergone peer review.
They should not be considered conclusive, used to inform clinical practice,
or referenced by the media as validated information.

Multi-model validation of the hydro-mechanical and soil–water characteristic behaviour of a slag-cement-amended iron ore tailings– bentonite liner material across compaction moisture states

B. O. Akinwande

akinwande.pg718093@st.futminna.edu.ng

Federal University of Technology

A. A. Amadi

Federal University of Technology

T. E. Adejumo

Federal University of Technology

H. S. Abdulrahman

Federal University of Technology

Research Article

Keywords: Landfill liner, Iron ore tailings, Bentonite, Slag cement, Moulding water content, Soil–water characteristic curve

Posted Date: November 6th, 2026

DOI: https://doi.org/10.21203/rs.3.rs-11418974/v1

License: This work is licensed under a Creative Commons Attribution 4.0 International License.
Read Full License

Additional Declarations: No competing interests reported.

Multi-model validation of the hydro-mechanical and soil–water characteristic behaviour of a slag-cement-amended iron ore tailings–bentonite liner material across compaction moisture states

B. O. Akinwande[1,*], A. A. Amadi[1], T. E. Adejumo[1], H. S. Abdulrahman[1]

[1] Department of Civil Engineering, Federal University of Technology, Minna, Nigeria

[*] Corresponding author: B. O. Akinwande, akinwande.pg718093@st.futminna.edu.ng

Author contributions

Conceptualization: B. O. Akinwande; Methodology: B. O. Akinwande; Investigation: B. O. Akinwande; Formal analysis: A. A. Amadi; Software: A. A. Amadi; Visualization: T. E. Adejumo; Supervision: T. E. Adejumo; Writing – original draft preparation: H. S. Abdulrahman; Writing – review and editing.

Abstract

Compacted liners made from iron ore tailings (IOT) and bentonite must satisfy strength, hydraulic and shrinkage criteria concurrently, yet these properties respond in opposing directions to the compaction water content. This study evaluates how the compaction moisture state (2% dry of optimum, DOPT; optimum, OPT; 2% wet of optimum, WOPT) governs the performance of IOT–bentonite mixtures (20–40% bentonite) stabilised with 0–10% slag cement (CEM III), compacted at British Standard Heavy (BSH) energy and cured for 28 days. Unconfined compressive strength (UCS), saturated hydraulic conductivity (K_{sat}) and volumetric shrinkage (V_s) were measured for 25 mixtures, and Gaussian process regression (GPR) was used to map the combined compliance region against UCS ≥ 200 kPa, $K_{sat} \leq 1 \times 10^{-9}$ m/s and $V_s \leq 4\%$. For the 30% bentonite/10% CEM III mixture, UCS decreased from 1775 to 1800 to 1542 kPa from DOPT to WOPT, K_{sat} from 1.37×10^{-9} to 1.93×10^{-10} to 9.73×10^{-11} m/s, and V_s from 3.8 to 3.19 to 2.19%. DOPT was therefore the only condition that violated the hydraulic criterion, despite giving the highest strength, whereas OPT and WOPT met all three criteria. Soil–water characteristic curves (SWCCs) measured by pressure plate up to 1500 kPa were fitted with the Brooks–Corey, Fredlund–Xing and van Genuchten models; all reproduced the data closely (root-mean-square error, RMSE ≤ 0.0035) and the van Genuchten model was marginally best. Water retention increased with moulding water content. 2%WOPT placement of a 31% bentonite/10% CEM III liner is recommended.

Keywords Landfill liner; Iron ore tailings; Bentonite; Slag cement; Moulding water content; Soil–water characteristic curve

1 Introduction

Mining operations worldwide generate very large volumes of iron ore tailings (IOT). Their storage in dams and stockpiles carries risks of dam failure, dust emission, land degradation and heavy-metal leachate migration into soils and water bodies (Abubakar et al. 2022; Vitor et al. 2023; Wu et al. 2026); beneficial reuse in earthworks and containment systems is therefore preferable to passive storage (Carmignano et al. 2021; Owolabi and Daramola 2024). IOT consists of fine particles rich in silica, alumina and iron oxides and is structurally stable, but it lacks the plasticity and low permeability needed for a stand-alone liner (Chao et al. 2024).

Compacted clay liners (CCLs) and geosynthetic clay liners (GCLs) are the conventional barrier options. However, uniform clay deposits are scarce in many geological settings and imported geosynthetics are often prohibitively expensive in developing regions (Mukiza et al. 2021; Kamaruddin et al. 2022; Aswathy and Sunil 2024). Sand–bentonite mixtures are a common alternative, but they depend on river sand, whose over-exploitation has serious ecological consequences. Blending a swelling clay such as sodium bentonite with a granular waste improves cohesion, workability and impermeability (Gupt et al. 2021; Eyo et al. 2021; Jain 2024; Raviteja et al. 2024), but bentonite-amended soils shrink strongly on

drying and are prone to desiccation cracking, which compromises barrier integrity and calls for stabilisation (Demdoum et al. 2020; Nath et al. 2023).

Slag cement is an attractive stabiliser produced by replacing part of the Portland clinker with ground granulated blast-furnace slag, which lowers the embodied carbon of the binder (Nie et al. 2022) and improves durability (Huynh and Van Ho 2025). Samani et al. (2020) showed that adding cement and bentonite to iron ore tailings raises the optimum moisture content and lowers the maximum dry density, yet still produces materials suitable for earthworks, depending on the binder and the moisture condition at compaction.

A soil liner must simultaneously provide adequate unconfined compressive strength (UCS) to resist construction and operational loads, a sufficiently low saturated hydraulic conductivity (K_{sat}) to restrict leachate migration, and limited volumetric shrinkage (V_s) to avoid desiccation cracking. Because these properties respond differently to the moulding water content, they must be assessed together. This idea underlies the "acceptable zone" concept, in which strength, hydraulic conductivity and shrinkage are evaluated across the compaction plane and a mix is acceptable only where all three criteria overlap (Daniel and Benson 1990; Osinubi and Nwaiwu 2006). The approach has been applied to lateritic soil–bentonite mixtures, where the compliant zone proved highly sensitive to both bentonite content and compaction water content (Amadi and Eberemu 2012).

Despite this body of work on lateritic soils, bentonite-amended clays and cement-treated tailings, little attention has been given to IOT–bentonite mixtures stabilised with slag cement. In particular, no study known to the authors has examined such a material across dry-of-optimum, optimum and wet-of-optimum moulding states while linking the saturated hydraulic response to the unsaturated water-retention behaviour. This study therefore (i) quantifies UCS, K_{sat} and V_s of 25 IOT–bentonite–slag-cement mixtures compacted at 2% dry of optimum, optimum and 2% wet of optimum; (ii) uses Gaussian process regression (GPR), a Bayesian non-parametric method valued for its uncertainty quantification in geotechnical applications (Zhang et al. 2022; Wu et al. 2024), to construct a "validity envelope" that delineates the feasible design space; (iii) identifies the moulding condition that best balances the three criteria; and (iv) compares the Brooks–Corey (BC), Fredlund–Xing (FX) and van Genuchten (vG) models for describing the soil–water characteristic curve (SWCC) of the selected mixture, to explain the observed moisture-state effects through pore-structure and suction behaviour.

2 Materials and methods

2.1 Materials

The IOT was collected from the National Iron Ore Mining Company, Itakpe, Kogi State, north-central Nigeria. A bulk sample was bagged for testing and a smaller portion was sealed in polythene to preserve the as-collected moisture content. At the Civil Engineering Soil Laboratory of the Federal University of Technology, Minna, the bulk sample was air-dried, pulverised and passed through a BS No. 4 sieve

(4.76 mm). Powdered sodium bentonite was obtained from a supplier in Kaduna, Nigeria. The slag cement (designated CEM III in this study) was produced by inter-grinding approximately 64% Portland clinker, 31% ground granulated blast-furnace slag and 5% gypsum in a laboratory ball mill, with most particles passing the 75 μm sieve (BSI 2011). The materials are shown in Fig. 1.



Fig. 1 Materials used: (top) raw and powdered blast-furnace slag; (bottom) Portland clinker, bentonite and iron ore tailings (IOT)

2.2 Mixture design and compaction

Twenty-five mixtures were prepared by adding bentonite at 20, 25, 30, 35 and 40% and CEM III at 0, 2.5, 5, 7.5 and 10% (percentages by dry mass of soil). Constituents were blended dry before hydration. Compaction followed BS 1377 (BSI 1990a) at British Standard Heavy (BSH) energy to represent high-energy field placement; the maximum dry density (MDD) and optimum moisture content (OMC) of each mixture were taken from its dry density–moisture content curve. The wet bulk density (ρ_b) and dry density (ρ_d) were computed from

$$\rho_b = \frac{M}{V} \tag{1}$$

$$\rho_d = \frac{\rho_b}{1+w} \tag{2}$$

where M is the mass of compacted soil (g), V the mould volume (cm^3) and w the moisture content (expressed as a fraction). The three moisture states used throughout the study were defined relative to each mixture's OMC: 2% dry of optimum (DOPT, OMC − 2%), optimum (OPT) and 2% wet of optimum (WOPT, OMC + 2%). Specimens for all tests were compacted at the corresponding moulding water content at BSH energy.

2.3 Consistency limits

Liquid limit (cone penetration method), plastic limit and plasticity index were determined in accordance with BS 1377 (BSI 1990a). The plasticity index was calculated as

$$\mathrm{PI} = \mathrm{LL} - \mathrm{PL} \tag{3}$$

where LL and PL are the liquid and plastic limits (%).

2.4 Unconfined compressive strength

Specimens were extruded, sealed and cured for 28 days before testing in a triaxial loading frame with zero confining pressure (Fig. 2a), following BS 1377 and BS 1924-2 (BSI 1990a, 1990b). A minimum UCS of 200 kPa was adopted as the liner criterion (Daniel and Wu 1993). The compressive stress was computed as

$$\sigma = \frac{RC_r(100-\varepsilon)}{100A_0} \tag{4}$$

$$\varepsilon(\%) = \left(\frac{v}{L_0}\right) \times 100 \tag{5}$$

where σ is the compressive stress (kN/m^2), R the load-ring reading, C_r the mean calibration factor of the ring, ε the axial strain (%), v the axial compression, L_0 the initial specimen length and A_0 the initial cross-sectional area.

2.5 Volumetric shrinkage

Specimens compacted at the three moisture states were extruded and air-dried on a laboratory bench at 25 ± 3 °C (Fig. 2b), and their dimensions were measured with a vernier caliper over 28 days. The volumetric shrinkage strain was calculated as

$$V_s = \left[\frac{V_i - V_f}{V_i}\right] \times 100 \tag{6}$$

where V_i is the initial volume and V_f the final (dry) volume. A limit of $V_s \leq 4\%$ was adopted (Daniel and Wu 1993).

2.6 Saturated hydraulic conductivity

Specimens compacted in rigid moulds as described above were cured for 28 days in a constant-humidity room (100% relative humidity, 18 °C), then saturated under a 1.0 m head of tap water for 4 days in a falling-head permeameter (Fig. 2c). Readings were continued until successive head measurements showed no significant difference at the equilibrium criteria of ASTM D5084 (ASTM International 2024). Hydraulic conductivity was computed from

$$K = \left[\frac{2.303aL}{A\Delta t}\right] \log_{10}\left(\frac{h_1}{h_2}\right) \tag{7}$$

where a is the standpipe cross-sectional area (m^2), L the specimen height (m), A the specimen cross-sectional area (m^2), Δt the elapsed time (s) and h_1, h_2 the initial and final standpipe heads (m). The criterion was $K_{sat} \leq 1 \times 10^{-9}$ m/s.

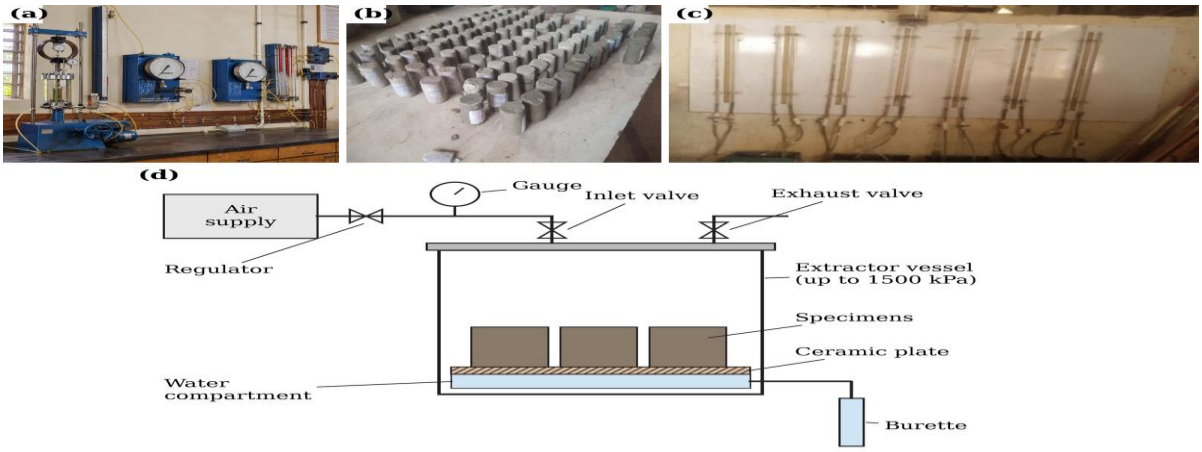


Fig. 2 Laboratory set-ups: (a) unconfined compression in the triaxial frame; (b) compacted specimens for shrinkage monitoring; (c) falling-head permeameter board; (d) schematic of the pressure plate set-up

2.7 Soil–water characteristic curves

SWCCs were determined by the pressure plate method (ASTM D6836) on four mixtures (25% bentonite/7.5% CEM III, 30%/7.5%, 30%/10% and 35%/10%) compacted at BSH energy at DOPT, OPT and WOPT, at matric suctions of 1, 10, 100, 500, 1000 and 1500 kPa. SWCC specimens were cured for 28 days. Detailed results are given for the 30% bentonite/10% CEM III mixture, which is the one examined for strength, shrinkage and hydraulic conductivity in Sections 3.4–3.8.

2.8 Statistical modelling and model evaluation

The responses Y (UCS, $\log_{10}K_{sat}$ and V_s) were related to the bentonite content B and CEM III content C by the second-order polynomial surface

$$Y = \beta_0 + \sum \beta_i X_i + \sum \beta_{ii} {X_i}^2 + \sum_{i<j} \beta_{ij} X_i X_j \tag{8}$$

with $X_1 = B$ and $X_2 = C$. A GPR surrogate with a radial basis function (RBF) kernel was used to map the non-linear response landscape, and its predictive accuracy was assessed by 5-fold cross-validation. The feasible region was defined as the intersection of the three constraints (UCS ≥ 200 kPa, $K_{sat} \le 1 \times 10^{-9}$ m/s, $V_s \le 4\%$), producing the "validity envelope". Goodness of fit was expressed by the coefficient of determination (R^2) and the root-mean-square error (RMSE):

$$R^2 = 1 - \frac{\sum (y_i - \hat{y}_i)^2}{\sum (y_i - \bar{y})^2} \tag{9}$$

$$\mathrm{RMSE} = \sqrt{\frac{1}{n}\sum (y_i - \hat{y}_i)^2} \tag{10}$$

The SWCC data were fitted with three models. The Brooks and Corey (1964) model is

$$\theta = \begin{cases} \theta_r + (\theta_s - \theta_r)\left(\frac{\psi}{\psi_b}\right)^{-\lambda}, & \text{for } \psi > \psi_b \\ \theta_s, & \text{for } \psi \le \psi_b \end{cases} \tag{11}$$

the Fredlund and Xing (1994) model (without the correction factor) is

$$\theta = \frac{\theta_s}{\left\{\ln\left[e+\left(\frac{\psi}{a}\right)^n\right]\right\}^m} \tag{12}$$

and the van Genuchten (1980) model is

$$\theta = \theta_r + \frac{(\theta_s-\theta_r)}{[1+(\alpha\psi)^n]^m},\ \ m = 1-\frac{1}{n} \tag{13}$$

where θ is the volumetric water content, ψ the matric suction (kPa), θ_s and θ_r the saturated and residual water contents, ψ_b the air-entry (bubbling) pressure and λ, a, n, m and α fitting parameters. Parameters were obtained by non-linear least squares with $\theta_r \geq 0$ and θ_s taken as the measured water content at 1 kPa. Fit quality was compared using RMSE, R^2 and the Akaike information criterion, AIC = N ln(SSE/N) + 2k, where N is the number of data points, SSE the sum of squared errors and k the number of parameters (Burnham and Anderson 2002).

3 Results and discussion

3.1 Material characterization

The physical properties of the three constituents are given in Table 1 and the grading curve of the IOT is shown in Fig. 3. The IOT is a poorly graded fine-to-medium sand (SP in the Unified Soil Classification System, USCS) of which only 3.72% passes the 0.075 mm sieve; its high specific gravity (3.32) reflects its iron-oxide-rich mineralogy. The smooth, narrow grading offers little interlocking and no cohesion, so the tailings alone cannot meet liner requirements. The bentonite is a highly plastic, expansive clay (CH) with a liquid limit of 301%, plasticity index of 259%, linear shrinkage of 38.4% and free swell of 102%, which explains both its sealing capacity and its tendency to shrink on drying. The slag cement is a fine powder (84.6% passing 0.075 mm) with a specific gravity of 2.99.

Table 1 Physical characteristics of the materials used

Property	IOT	Bentonite	CEM III
Retained on No. 200 sieve (> 0.075 mm) (%)	96.28	–	–
Passing No. 200 sieve (< 0.075 mm) (%)	3.72	–	84.6
Liquid limit (%)	24.2	301	–
Plastic limit (%)	NP	42	–
Plasticity index (%)	NP	259	–
Linear shrinkage (%)	3.6	38.4	–
Specific gravity	3.32	2.59	2.99
Free swell (%)	–	102	–
USCS class	SP	CH	–

NP = non-plastic; – = not determined; USCS = Unified Soil Classification System; SP = poorly graded sand; CH = high-plasticity clay

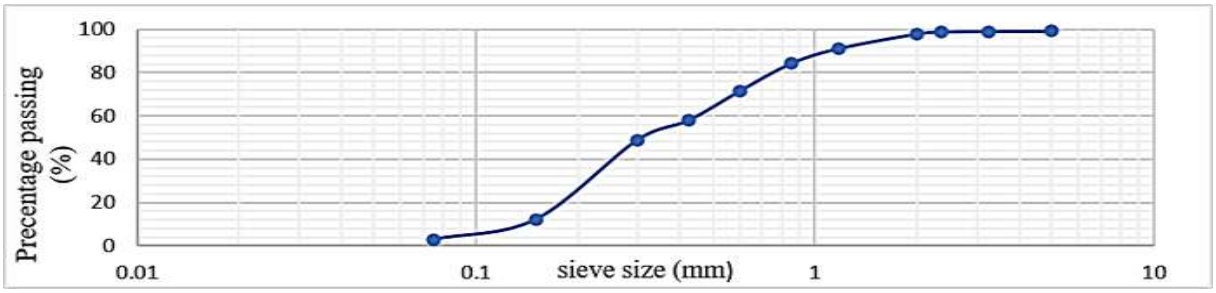


Fig. 3 Particle-size distribution of the iron ore tailings (IOT)

Oxide compositions are listed in Table 2. SiO_2 + Al_2O_3 + Fe_2O_3 amount to 96.49% of the IOT, above the 70% minimum used in ASTM C618 (ASTM International 2025) to identify pozzolanic materials, although actual reactivity depends on the amorphous fraction, which was not determined here. The bentonite is dominated by silica and alumina (63.34% and 23.68%), consistent with a smectitic clay. The slag cement contains 53.25% CaO, the source of the calcium hydroxide and calcium silicate hydrate that drive cementation and pozzolanic reaction with the silica- and alumina-bearing IOT and bentonite.

Table 2 Oxide composition of the materials used (% by mass)

Material	SiO_2	Al_2O_3	MgO	Na_2O	Fe_2O_3	CaO	P_2O_5	K_2O	TiO_2	MnO
IOT	26.93	2.75	0.45	–	66.81	0.63	–	–	0.16	0.02
Bentonite	63.34	23.68	2.51	1.98	2.03	1.11	0.12	0.63	1.76	0.05
CEM III	1.40	25.51	0.31	0.03	10.55	53.25	0.13	0.05	0.03	0.01

3.2 Consistency limits

The liquid limit (Fig. 4) increased with bentonite content at every CEM III dosage, from 27.9% at 20% bentonite to 29.5% at 40% bentonite without cement. Adding CEM III raised the liquid limit further, reaching 38.5% at 40% bentonite and 10% CEM III. All mixtures therefore exceeded the minimum liquid limit of 20% commonly specified for liner materials. The plasticity index also rose with cement content, from 11.5% to 18.5% at 40% bentonite as CEM III increased from 0 to 10%, so the plastic range widened rather than narrowed. This is contrary to the usual effect of cement or lime on clays. It may reflect flocculation and agglomeration of bentonite by calcium released during slag-cement hydration, which increases the water-holding capacity of the fabric (Kumar and Kumari 2024), but this explanation was not tested by microstructural analysis in the present work. Because some of the cement-treated mixtures exceeded the upper plasticity index bound of 12% sometimes quoted for liners while still meeting the K_{sat} and V_s criteria, the plasticity index was not treated as a governing criterion.

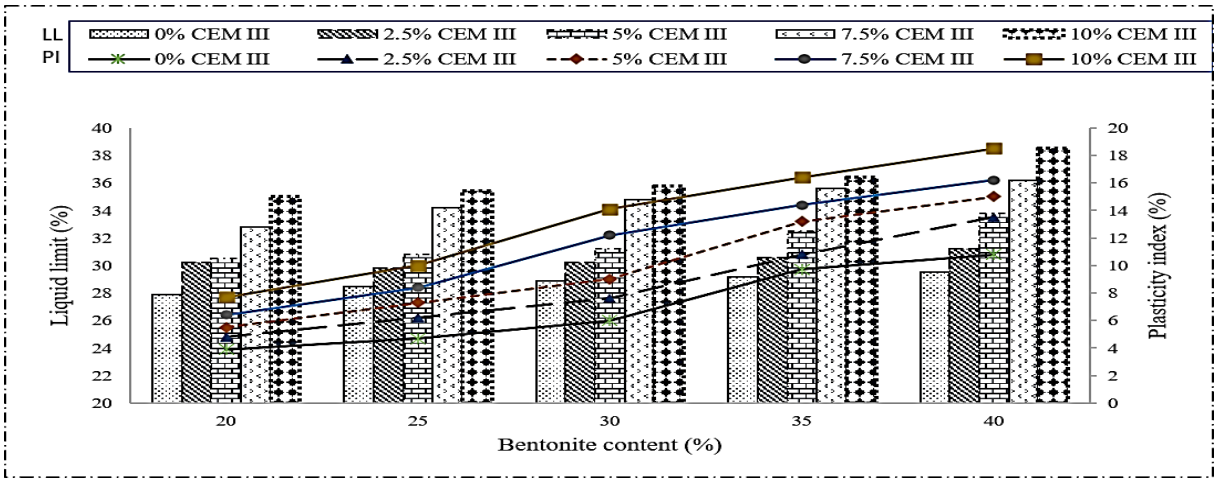


Fig. 4 Variation of liquid limit (bars) and plasticity index (lines) with bentonite and CEM III content

3.3 Compaction characteristics

Compaction results are summarized in Table 3. The MDD decreased with bentonite content, from 2.19 g/cm^3 at 20% bentonite to 2.07 g/cm^3 at 40% bentonite without cement, owing to the lower specific gravity and higher water affinity of bentonite. The MDD increased with CEM III, from 2.19 to 2.31 g/cm^3 at 20% bentonite as cement rose from 0 to 10%, consistent with the higher specific gravity of the cement and the formation of calcium silicate hydrate, which improves particle packing (Ghazi 2015; Amadi et al. 2025). The OMC showed the opposite trend, rising with both bentonite and cement content: from 17.2% at 20% bentonite to 18.2% at 40% bentonite without cement, and from 18.2% to 19.5% at 40% bentonite as cement increased from 0 to 10%. The higher water demand is attributable to cement hydration and to the greater surface area of flocculated and agglomerated particles (Ghadr and Assadi-Langroudi 2018; Amadi et al. 2025).

Table 3 Maximum dry density (MDD, g/cm^3) and optimum moisture content (OMC, %) of the mixtures at BSH energy

Bentonite (%)	0% CEM III		2.5% CEM III		5% CEM III		7.5% CEM III		10% CEM III	
	MDD	OMC	MDD	OMC	MDD	OMC	MDD	OMC	MDD	OMC
20	2.19	17.2	2.21	17.4	2.25	17.5	2.28	17.9	2.31	18.2
25	2.15	17.3	2.18	17.5	2.21	17.8	2.25	18.1	2.28	18.5
30	2.12	17.5	2.15	17.9	2.18	18.2	2.23	18.5	2.25	18.7
35	2.09	17.7	2.13	18.1	2.16	18.5	2.19	18.8	2.21	19.1
40	2.07	18.2	2.09	18.5	2.12	18.9	2.16	19.1	2.19	19.5

3.4 Unconfined compressive strength

Unconfined compressive strength, UCS at the three moisture states is presented in Fig. 5. Strength increased with CEM III content at every bentonite level and peaked at 30% bentonite for all cement contents; beyond 30% bentonite it declined. For example, UCS increased from 752, 680 and 520 kPa (DOPT, OPT, WOPT) at 20% bentonite/0% CEM III to peak values of 1775, 1800 and 1542 kPa at 30% bentonite/10% CEM III, and decreased to 1400, 1295 and 1225 kPa at 40% bentonite/10% CEM III. The gain with cement is attributed to the pozzolanic reaction between the lime liberated by cement

hydration and the silica and alumina-bearing IOT and bentonite, which forms secondary cementitious products. The decline at higher bentonite contents is consistent with a dilution of the cementing action by the increasing volume of expansive clay and with its higher water demand.

UCS decreased as the moulding water content increased, reflecting a shift from a flocculated, cement- and clay-bridged fabric on the dry side to a more dispersed and weaker fabric on the wet side (Lambe 1958; Seed and Chan 1959). All mixtures at 10% CEM III exceeded the 200 kPa criterion (Daniel and Wu 1993; Ghazi 2015; Kuranchie et al. 2015) by a wide margin: the 30% bentonite/10% CEM III mixture exceeded it 8.9, 8.6 and 7.7 times at DOPT, OPT and WOPT, respectively.

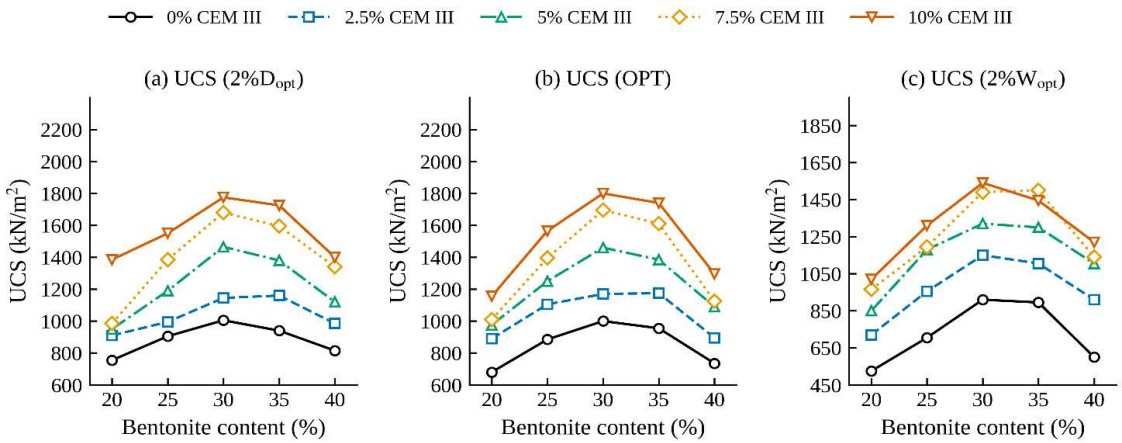


Fig. 5 UCS of cemented IOT–bentonite mixtures at (a) 2% dry of optimum, (b) optimum and (c) 2% wet of optimum. Mixtures with UCS ≥ 200 kPa satisfy the liner requirement

3.5 Volumetric shrinkage

Volumetric shrinkage is shown in Fig. 6. Adding CEM III reduced V_s at all bentonite contents, whereas increasing the bentonite content generally increased it. At 10% CEM III, V_s stayed at or below about 4% for all bentonite contents, while several mixtures with 0–5% CEM III and 35–40% bentonite exceeded the 4% limit. For the 30% bentonite/10% CEM III mixture, V_s was 3.8%, 3.19% and 2.19% at DOPT, OPT and WOPT, respectively, equivalent to about 80%, 80% and 55% of the allowable limit. Volumetric shrinkage at this composition was therefore governed mainly by the bentonite and cement contents, with a clear reduction only on the wet side. These values were obtained by unconfined air-drying of single specimens for 28 days with caliper measurements (Albrecht and Benson 2001).

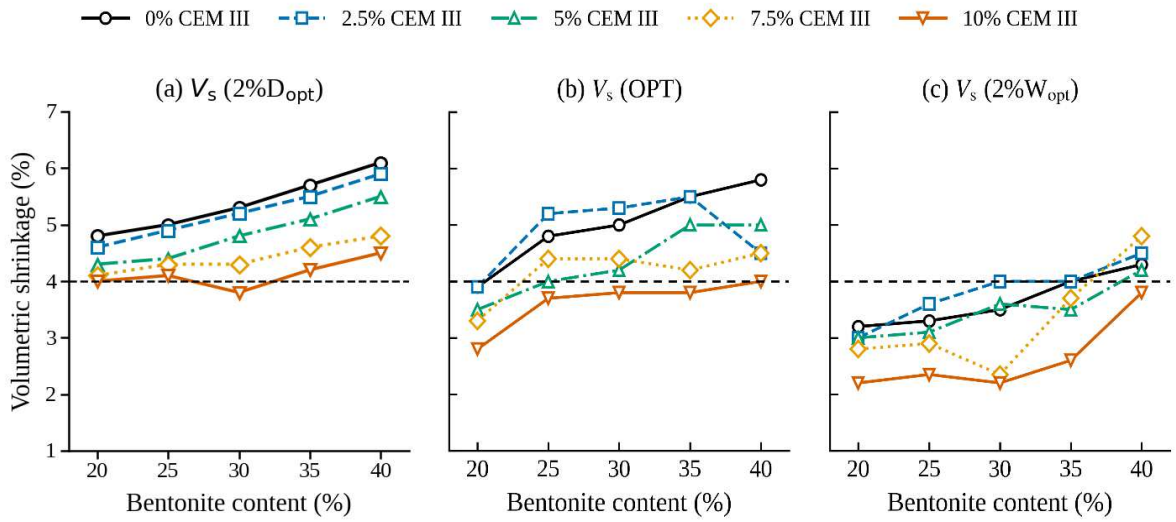


Fig. 6 V_s of IOT–bentonite mixtures treated with slag cement at (a) 2% dry of optimum, (b) optimum and (c) 2% wet of optimum. The dashed line is the 4% limit

3.6 Saturated hydraulic conductivity

Saturated hydraulic conductivity, K_{sat} results are shown in Fig. 7. Without cement, all mixtures had K_{sat} of the order of 10^{-8} m/s at every moisture state and failed the 1×10^{-9} m/s criterion, even at 40% bentonite. For cement-treated mixtures, K_{sat} decreased with bentonite content up to about 30–35% and then rose again at 40%, mirroring the UCS peak and possibly reflecting the greater shrinkage of the high-bentonite mixtures. Cement addition lowered K_{sat} by roughly 1.3 to 2.3 orders of magnitude at 30% bentonite: from about 3×10^{-8}, 3×10^{-8} and 1.6×10^{-8} m/s without cement to 1.37×10^{-9}, 1.93×10^{-10} and 9.73×10^{-11} m/s at 10% CEM III for DOPT, OPT and WOPT, respectively. Only the DOPT specimen therefore exceeded the limit (by a factor of 1.4), whereas the OPT and WOPT specimens were 5 and 10 times below it. The beneficial effect of additional moulding water is consistent with improved bentonite hydration and swelling, which clogs the larger pores and reduces hydraulic conductivity. Similar behaviour has been reported for compacted tailings–bentonite and slag- or pozzolan-stabilised barrier materials (Osinubi and Amadi 2010; Osinubi et al. 2015; Osinubi et al. 2019; Amadi and Eberemu 2012; Okoro et al. 2023).

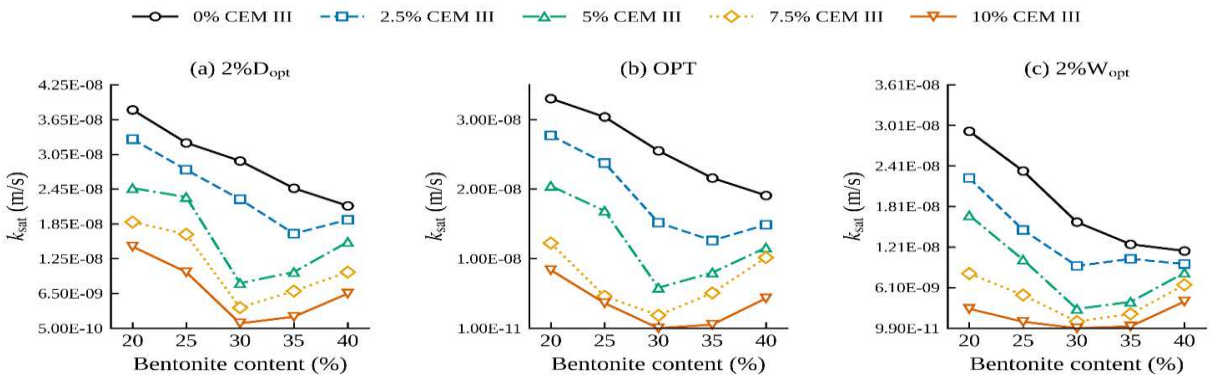


Fig. 7 K_{sat} of IOT–bentonite mixtures treated with slag cement at (a) 2% dry of optimum, (b) optimum and (c) 2% wet of optimum. Mixtures with $K_{sat} \leq 1 \times 10^{-9}$ m/s satisfy the liner requirement

3.7 Effect of moulding water content on the design criteria

The effect of moulding water content on the three criteria for the 30% bentonite/10% CEM III mixture is summarised in Fig. 8 and Table 4. Linear trend lines were fitted to the three experimental points of each property against relative moulding water content. Because only three moisture states were tested, these fits have a single degree of freedom and describe the direction and approximate magnitude of the trends rather than statistically established relationships; the GPR predictions in Fig. 8 merely interpolate between them.

UCS decreased by about 58 kPa per 1% increase in moulding water content (R^2 = 0.915), in line with the classical fabric argument that clay compacted dry of optimum is flocculated and that compacted wet of optimum is dispersed (Lambe 1958; Seed and Chan 1959). K_{sat} fell steadily with water content (R^2 = 0.928): each 1% increase reduced K_{sat} by a factor of about 1.9, so the value fell roughly 14-fold across the 4% span from DOPT to WOPT. The fitted line crosses the 1×10^{-9} m/s limit at about 1.8% dry of optimum, i.e. the DOPT specimen failed by a narrow margin. This is the usual behaviour of compacted clay: wet-side compaction produces a more dispersed fabric with smaller, better-connected pores, and the low-permeability zone is conventionally located on the water-content–dry-density plane (Daniel and Benson 1990). Amadi and Eberemu (2012) applied the same limit to lateritic soil–bentonite mixtures compacted dry, at and wet of optimum, and Okoro et al. (2023) selected 2% wet of optimum for their iron-ore-tailings–bentonite durability tests, both consistent with the present K_{sat} results.

V_s decreased by 0.255 percentage points per 1% increase in water content, but the fit is weaker (R^2 = 0.765) and the change is concentrated between OPT and WOPT (3.19% to 2.19%), with noticeable difference between DOPT and OPT (3.8% and 3.19%) (Albrecht and Benson 2001; Daniel and Wu 1993). A possible explanation is that the greater hydration of bentonite and cement at the higher water content develops a more coherent matrix that resists shrinkage.

Table 4 Design-criterion values and linear trends with moulding water content for the 30% bentonite/10% CEM III mixture

Property	DOPT	OPT	WOPT	Limit	Trend per +1% water content	R^2 (n = 3)
UCS (kPa)	1775	1720	1542	≥ 200	−58.25 kPa	0.915
K_{sat} (m/s)	1.37×10^{-9}	1.93×10^{-10}	9.73×10^{-11}	≤ 1×10^{-9}	$\log_{10} K_{sat} = -0.287\, w - 9.530$ (÷ 1.94)[a]	0.928
V_s (%)	3.21	3.19	2.19	≤ 4	−0.255 percentage points	0.765
Compliance	Fails K_{sat}	Passes all	Passes all			

w is the moulding water content relative to optimum (%)

[a] Log-linear fit; "÷ 1.94" indicates that K_{sat} falls by a factor of 1.94 per +1% water content

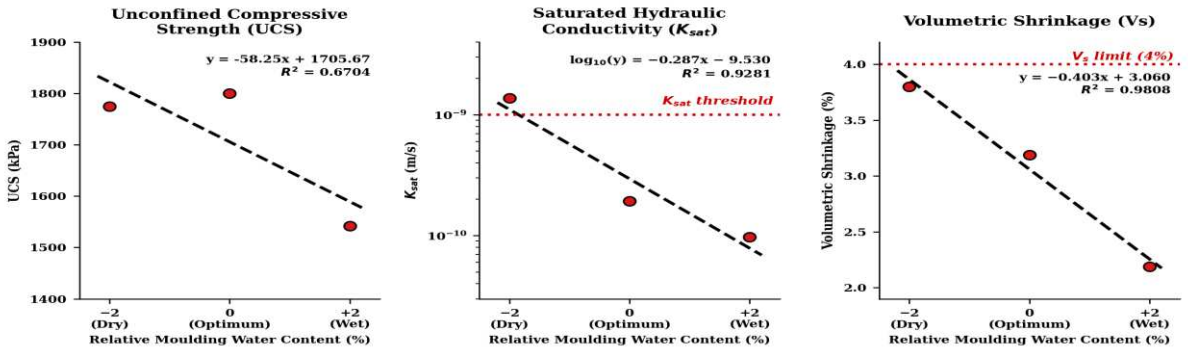


Fig. 8 Trends of UCS, K_{sat} and V_s with relative moulding water content for the 30% bentonite/10% CEM III mixture (red: experimental; blue: GPR predictions; dashed: linear trend)

3.8 Validity envelope

The validity envelope (Fig. 9) combines the three constraints, UCS ≥ 200 kPa, $K_{sat} \leq 1 \times 10^{-9}$ m/s and $V_s \leq 4\%$, into the region of bentonite and cement contents that satisfy all of them. The UCS response surface at OPT is

$$\mathrm{UCS} = -2910.13 + 262.69B + 60.19C - 4.34B^2 + 0.76BC - 1.72C^2 \qquad (14)$$

with B and C in per cent and UCS in kPa. The lower bound of the compliant region corresponded to bentonite contents of 34.2%, 22.8% and 27.7% at DOPT, OPT and WOPT, respectively, with a minimum CEM III content of 7.8%. Numerical optimisation identified 31.1% bentonite and 10% CEM III as the optimum mix; this is the point at which the UCS surface is maximised for 10% CEM III, and because 10% is the upper limit of the tested cement range it is a boundary solution whose extrapolation beyond 10% was not examined. The nearest tested mixture, 30% bentonite/10% CEM III, gave the lowest K_{sat} (9.73×10^{-11} m/s) and V_s (2.19%) at WOPT, both well inside the limits, while retaining UCS of 1542 kPa.

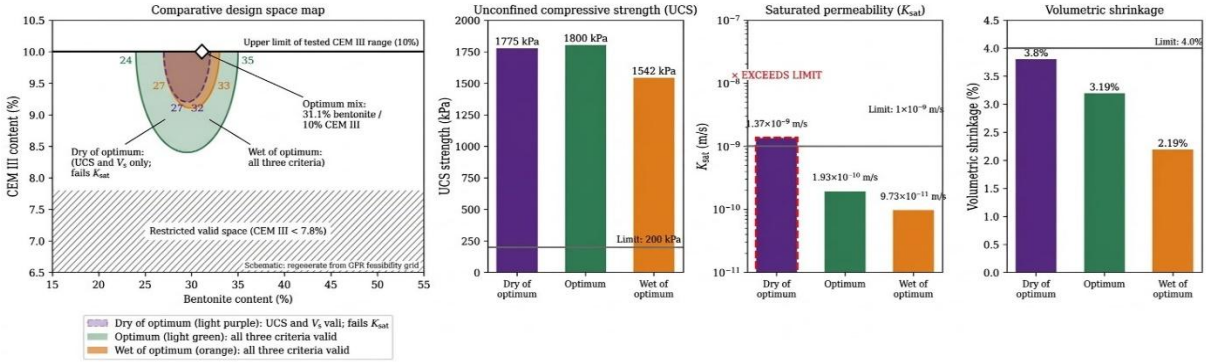


Fig. 9 Validity envelope and comparison of UCS, K_{sat} and V_s at the three moisture states for IOT–bentonite mixtures treated with slag cement

3.9 Soil–water characteristic behaviour

While K_{sat} describes the response under saturated conditions, the pore structure that controls it also governs water retention under suction. SWCCs were therefore measured at the three moisture states

and fitted with the BC, FX and vG models (Eqs. (11)–(13)); detailed results are presented for the 30% bentonite/10% CEM III mixtures.

3.9.1 Model performance

All three models reproduced the measured data very closely (Table 5): the average RMSE was 0.0032 for BC and vG and 0.0035 for FX, and the average R^2 was 0.9987–0.9988. The vG model gave the lowest average AIC (−62.09), but the differences from BC (−61.77) and FX (−60.62) are below 2 units, so the models are statistically indistinguishable on this criterion. This must be interpreted with caution, because each curve comprises only six measurements fitted with three parameters (θ_s being taken from the measurement at 1 kPa), leaving only three degrees of freedom, and the fits therefore approach interpolation. Table 6 compares measured and predicted water contents: the differences were mostly smaller than 0.002, and BC was closest at five of the nine points at 500–1500 kPa, vG at three, with the remaining point shared between them. All models predicted a flat plateau at 1–10 kPa (e.g. 0.3813 at DOPT), slightly overestimating the measured value at 10 kPa (0.3747), which indicates the onset of desaturation at lower suction than the models represent. The OPT entries at 1000 and 1500 kPa are identical for the measurements and for all three models.

Table 5 Overall fit performance of the SWCC models across all fitted curves

Model	Avg. RMSE	Min. RMSE	Max. RMSE	Avg. R^2	Avg. AIC	Rank (AIC)
Brooks–Corey	0.0032	0.0020	0.0082	0.9988	−61.77	2
Fredlund–Xing	0.0035	0.0020	0.0083	0.9987	−60.62	3
van Genuchten	0.0032	0.0020	0.0082	0.9988	−62.09	1

Table 6 Measured and predicted volumetric water content at each matric suction

Condition	Suction (kPa)	Lab	FX	vG	BC	Closest to lab
DOPT	1	0.3813	0.3813	0.3813	0.3813	Equal
	10	0.3747	0.3813	0.3813	0.3813	Equal
	100	0.3493	0.3493	0.3493	0.3493	Equal
	500	0.1783	0.1794	0.1785	0.1782	BC
	1000	0.1617	0.1623	0.1609	0.1618	BC
	1500	0.1569	0.1552	0.1574	0.1568	BC
OPT	1	0.3980	0.3980	0.3980	0.3980	Equal
	10	0.3910	0.3980	0.3979	0.3980	Equal
	100	0.3633	0.3633	0.3633	0.3633	Equal
	500	0.1877	0.1890	0.1878	0.1875	vG
	1000	0.1703	0.1712	0.1699	0.1708	vG
	1500	0.1703	0.1712	0.1699	0.1708	vG
WOPT	1	0.4143	0.4143	0.4143	0.4143	Equal
	10	0.4050	0.4143	0.4142	0.4143	Equal
	100	0.3750	0.3749	0.3749	0.3750	BC
	500	0.2003	0.2016	0.2005	0.2001	vG / BC
	1000	0.1807	0.1814	0.1801	0.1811	BC
	1500	0.1750	0.1730	0.1754	0.1748	BC

"Equal" indicates that the three models gave the same predicted value to within 0.0001. DOPT, OPT and WOPT: 2% dry of optimum, optimum and 2% wet of optimum

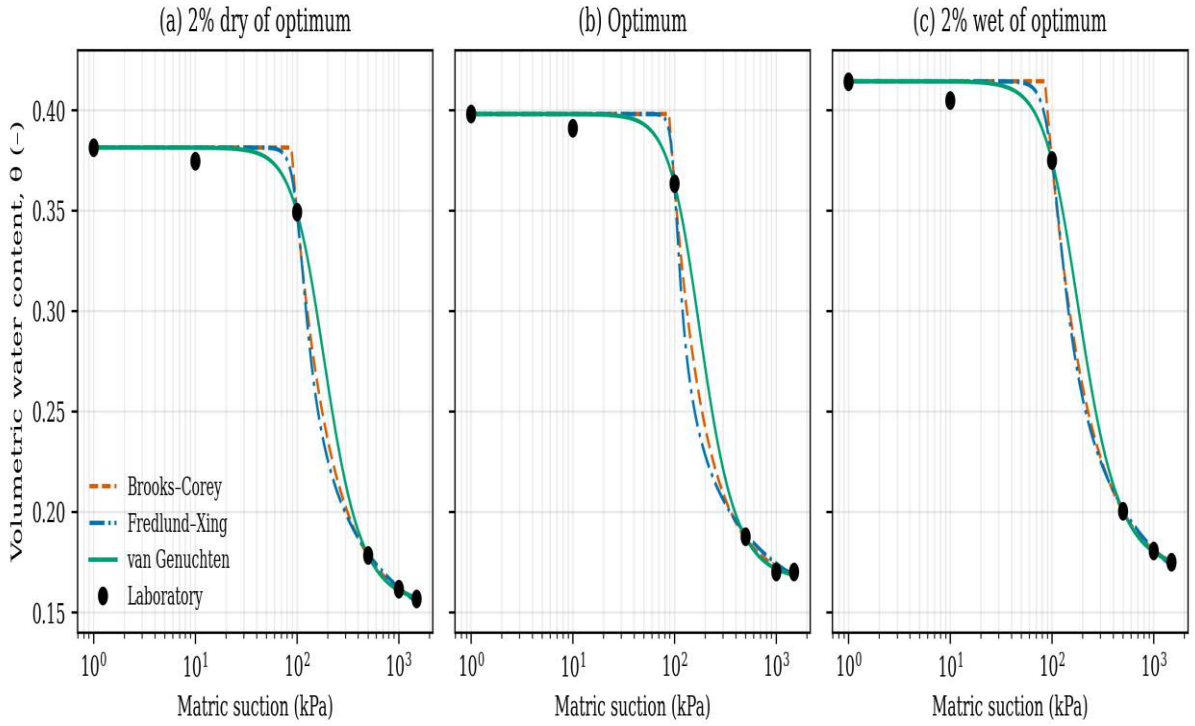


Fig. 10 Measured SWCC data and fitted BC, FX and vG curves for the 30% bentonite/10% CEM III mixture compacted at (a) 2% dry of optimum, (b) optimum and (c) 2% wet of optimum. Curves are drawn from the parameters in Table 7

3.9.2 Water retention and pore structure

In all three mixtures, the water content was nearly constant from saturation to a suction of about 100 kPa, consistent with an air-entry value of the order of 100 kPa (the fitted BC bubbling pressures are 86–89 kPa and $1/\alpha$ of the vG fits is 151–158 kPa; Table 7). Between 100 and 500 kPa the water content dropped sharply, by about 0.17 in each mixture, and about 90% of the water released between 1 and 1500 kPa had drained by 500 kPa, after which the curves flattened towards the residual value. At higher suction, water retention is controlled increasingly by adsorption and mineralogy rather than pore-size distribution, which is why the curves converge in shape.

Moulding water content shifted the curves upward without changing their form. The near-saturated water content increased from 0.3813 at DOPT to 0.398 at OPT and 0.4143 at WOPT, and the water content at 1500 kPa increased from 0.157 to 0.170 and 0.175. Higher retention at every suction on the wet side indicates greater hydration of the bentonite and a larger fraction of adsorbed and micro-pore water. The WOPT specimen has the highest saturated water content and is therefore not the densest, yet it has the lowest K_{sat}. This suggests that hydraulic conductivity is controlled by the continuity of the larger pores rather than by total porosity: compaction on the dry side leaves inter-aggregate macropores that form preferential flow paths, whereas wet-side compaction remoulds the clods and allows swollen bentonite to seal those paths (Daniel and Benson 1990; Vanapalli et al. 1999).

The SWCC results also help to explain the shrinkage behaviour. Drying produces suction, and the volume change it causes depends on how much clay-bound water is available and how stiff the cemented matrix is. The wet-side specimens hold more water at a given suction and, with fully hydrated bentonite and cement, can resist the capillary stresses that develop on drying, which is consistent with the lowest V_s (2.19%) at WOPT. Conversely, the dry-side specimens, with less hydrated bentonite and more open macropores, showed higher K_{sat} and marginally higher V_s (3.21% against 3.19% at OPT). Detailed SWCC results are given for a single mixture, so the effect of bentonite content on retention is not discussed here.

3.9.3 Choice of SWCC model

Because the three models fit equally well, the choice should rest on engineering usefulness. The vG model is recommended for this material. It had the lowest average AIC and RMSE (tied with BC), it is smooth and continuous through the air-entry region whereas BC has a discontinuity at ψ_b, and its closed-form coupling with the Mualem (1976) model gives the unsaturated hydraulic conductivity function directly, which is needed to assess the unsaturated performance of a liner or cover. The FX exponent n was poorly constrained (8.9, 15.0 and 6.7 at DOPT, OPT and WOPT, respectively; Table 7): the OPT value lies at the upper bound of 15, and the DOPT and WOPT values change markedly with the starting values. BC remains a useful alternative for the high-suction region, where it was closest to the measurements most often, and it provides a physically direct estimate of the air-entry value.

Table 7 Fitted SWCC model parameters for the 30% bentonite/10% CEM III mixture

Model	Parameter	DOPT	OPT	WOPT
All models	θ_s (measured at 1 kPa)	0.3813	0.3980	0.4143
Brooks–Corey	θ_r	0.1490	0.1640	0.1641
	ψ_b (kPa)	88.3	88.8	85.6
	λ	1.196	1.345	1.098
Fredlund–Xing	a (kPa)	98.0	96.6	96.0
	n	8.94	15.0[a]	6.68
	m	0.2815	0.2321	0.3002
van Genuchten	θ_r	0.1545	0.1662	0.1710
	α (kPa^{-1})	0.00631	0.00651	0.00661
	n	2.934	3.011	2.747
	$m = 1 - 1/n$	0.659	0.668	0.636

3.10 Practical implications and limitations

Taken together, the results indicate that a 30–31% bentonite/10% CEM III mixture satisfies all three liner criteria when compacted at OPT or WOPT, and fails only the hydraulic criterion at DOPT. WOPT is recommended as the target placement condition because it gave the lowest K_{sat}, the lowest V_s and the highest water retention, and because strength remained 7.7 times the minimum. The choice carries a trade-off: UCS was 13% lower than at DOPT, and wet-side placement is more demanding in the field

(trafficability, control of moisture), so a placement window from OPT to 2% wet of optimum is advisable. The following limitations should be noted: (i) detailed SWCC results are for one mixture; (ii) all tests were conducted at a single curing age of 28 days; (iii) shrinkage was measured by unconfined air-drying without wet–dry cycling; (iv) hydraulic conductivity was measured with tap water rather than leachate, in rigid-wall permeameters; (v) the trend fits across moulding states rest on three points; and (vi) the 10% CEM III content lies at the boundary of the tested range.

4 Conclusions

1. For the 30% bentonite/10% CEM III mixtures, UCS decreased with moulding water content (1775, 1800 and 1542 kPa at DOPT, OPT and WOPT), but remained 7.7–8.9 times the 200 kPa minimum. The roughly 13% strength loss across the 4% water content range is modest relative to this reserve.
2. Saturated hydraulic conductivity decreased by a factor of about 1.9 per 1% increase in moulding water content, from 1.37×10^{-9} (DOPT) to 1.93×10^{-10} (OPT) and 9.73×10^{-11} m/s (WOPT). Only DOPT exceeded the 1×10^{-9} m/s limit; OPT and WOPT were about 5 and 10 times below it.
3. Volumetric shrinkage was 3.8%, 3.19% and 2.19% at DOPT, OPT and WOPT, all below the 4% limit. CEM III reduced shrinkage at all bentonite contents.
4. The validity envelope, built from GPR surfaces, identified 31.1% bentonite and 10% CEM III as the optimum mix, with 30% bentonite/10% CEM III as the nearest tested and validated composition. The optimum lies at the upper boundary of the tested cement range.
5. SWCCs showed negligible desaturation up to about 100 kPa, rapid water loss between 100 and 500 kPa, and higher water retention with increasing moulding water content. The BC, FX and vG models all fitted closely; vG is recommended for its smoothness and its direct link to the unsaturated hydraulic conductivity function.
6. Placement at 2% wet of optimum is recommended for a 30–31% bentonite/10% CEM III liner, with a practical window from optimum to 2% wet of optimum. Further work should address wet–dry cycling, permeation with leachate, additional curing ages and SWCCs for other mixtures.

Statements and Declarations

Funding The authors did not receive support from any organization for the submitted work.

Competing interests The authors have no relevant financial or non-financial interests to disclose.

Data availability The datasets generated and analyzed during the current study are available from the corresponding author on reasonable request.

Use of AI-assisted technology During the preparation of this work the authors used Claude (Anthropic) to improve language and readability. After using this tool, the authors reviewed and edited the content as needed and take full responsibility for the content of the published article.

References

Abubakar IR, Maniruzzaman KM, Dano UL, AlShihri FS, AlShammari MS, Ahmed SMS, Alrawaf TI (2022) Environmental sustainability impacts of solid waste management practices in the global South. Int J Environ Res Public Health 19(19):12717

Albrecht BA, Benson CH (2001) Effect of desiccation on compacted natural clays. J Geotech Geoenviron Eng 127(1):67–75. https://doi.org/10.1061/(ASCE)1090-0241(2001)127:1(67)

Amadi AA, Eberemu AO (2012) Delineation of compaction criteria for acceptable hydraulic conductivity of lateritic soil–bentonite mixtures designed as landfill liners. Environ Earth Sci 67(4):999–1006. https://doi.org/10.1007/s12665-012-1544-z

Amadi AA, Kolo SS, Yusuf A, Eze FE, Salihu U (2025) Stabilization characteristics of cemented lateritic soil produced with selected cement types. Cement 19:100136. https://doi.org/10.1016/j.cement.2025.100136

ASTM International (2024) Standard test methods for measurement of hydraulic conductivity of saturated porous materials using a flexible wall permeameter (ASTM D5084-24). https://doi.org/10.1520/D5084-24

ASTM International (2025) Standard specification for coal ash and raw or calcined natural pozzolan for use in concrete (ASTM C618-25). https://doi.org/10.1520/C0618-25

Aswathy CM, Sunil BM (2024) Improving landfill liner performance with bentonite slag blend permeated with ammonia for a municipal solid waste landfill. J Environ Manage 367:122013. https://doi.org/10.1016/j.jenvman.2024.122013

Brooks RH, Corey AT (1964) Hydraulic properties of porous media. Hydrology Paper No. 3, Colorado State University, Fort Collins

BSI (1990a) Methods of test for soils for civil engineering purposes (BS 1377:1990). British Standards Institution, London

BSI (1990b) Stabilized materials for civil engineering purposes: methods of test for cement-stabilized and lime-stabilized materials (BS 1924-2:1990). British Standards Institution, London

BSI (2011) Cement. Composition, specifications and conformity criteria for common cements (BS EN 197-1:2011). British Standards Institution, London

Burnham KP, Anderson DR (2002) Model selection and multimodel inference: a practical information-theoretic approach, 2nd edn. Springer, New York

Carmignano OR, Vieira SS, Teixeira APC, Lameiras FS, Brandão PRG, Lago RM (2021) Iron ore tailings: characterization and applications. J Braz Chem Soc 32:1895–1911. https://doi.org/10.21577/0103-5053.20210100

Chao X, Han C, Shao C, Wang C, Wen P, Wang C (2024) Recent advances in properties and application progress of cement-based materials with iron tailing. Sustainability 16(23):10631. https://doi.org/10.3390/su162310631

Daniel DE, Benson CH (1990) Water content–density criteria for compacted soil liners. J Geotech Eng 116(12):1811–1830. https://doi.org/10.1061/(ASCE)0733-9410(1990)116:12(1811)

Daniel DE, Wu Y-K (1993) Compacted clay liners and covers for arid sites. J Geotech Eng 119(2):223–237. https://doi.org/10.1061/(ASCE)0733-9410(1993)119:2(223)

Demdoum A, Gueddouda MK, Goual I, Souli H, Ghembaza MS (2020) Effect of landfill leachate on the hydromechanical behavior of bentonite-geomaterials mixture. Constr Build Mater 234:117356

Eyo E, Abbey S, Oti J, Ng'ambi S, Ganjian E, Coakley E (2021) Microstructure and physical-mechanical characteristics of treated kaolin-bentonite mixture for application in compacted liner systems. Sustainability 13(4):1617. https://doi.org/10.3390/su13041617

Fredlund DG, Xing A (1994) Equations for the soil-water characteristic curve. Can Geotech J 31(4):521–532. https://doi.org/10.1139/t94-061

Ghadr S, Assadi-Langroudi A (2018) Structure-based hydro-mechanical properties of sand-bentonite composites. Eng Geol. https://doi.org/10.1016/j.enggeo.2018.02.002

Ghazi AF (2015) Engineering characteristics of compacted sand-bentonite mixtures. Dissertation, Edith Cowan University. http://ro.ecu.edu.au/theses/1615

Gupt CB, Bordoloi S, Sahoo RK, Sekharan S (2021) Mechanical performance and micro-structure of bentonite-fly ash and bentonite-sand mixes for landfill liner application. J Clean Prod 292:126033

Huynh TP, Van Ho Q (2025) Systematic assessment of the technical performance, durability, cost, and environmental impact of sustainable concrete incorporating fly ash and ground granulated blast-furnace slag. Environ Prog Sustain Energy 44(5):e70050

Jain AK (2024) Exploring the viability of bentonite-amended blends incorporating marble dust, sand, and fly ash for the creation of an environmentally sustainable landfill liner system. Int J Geo-Eng 15(1):16

Kamaruddin MA, Norashiddin FA, Yusoff MS, Hanif MHM, Wang LK, Wang MHS (2022) Sanitary landfill operation and management. In: Solid waste engineering and management, vol 1, pp 525–575

Kumar R, Kumari S (2024) Exploring the geotechnical and microstructural properties of composite mixtures for landfill liner materials: an experimental investigation. Environ Sci Pollut Res 31(22):33011–33029

Kuranchie FA, Shukla SK, Habibi D, Mohyeddin A (2015) Utilisation of iron ore tailings as aggregates in concrete. Mater Des 65:1162–1170

Lambe TW (1958) The structure of compacted clay. J Soil Mech Found Div 84(2):1–34. https://doi.org/10.1061/JSFEAQ.0000114

Mualem Y (1976) A new model for predicting the hydraulic conductivity of unsaturated porous media. Water Resour Res 12(3):513–522. https://doi.org/10.1029/WR012i003p00513

Mukiza E, Zhang L, Liu X, Zhang N (2021) Utilization of iron ore tailings as a base material in geotechnical engineering applications: a review. Constr Build Mater 282

Nath H, Kabir MH, Al Kafy A, Rahaman ZA, Rahman MT (2023) Geotechnical properties and applicability of bentonite-modified local soil as landfill and environmental sustainability liners. Environ Sustain Indic 18:100241

Nie S, Zhou J, Yang F, Lan M, Li J, Zhang Z, Sanjayan JG (2022) Analysis of theoretical carbon dioxide emissions from cement production: methodology and application. J Clean Prod 334:130270

Okoro IJ, Amadi AA, Alhassan M (2023) Hydraulic conductivity characteristics of iron-ore tailings–bentonite mixtures exposed to landfill leachate. J Hazard Toxic Radioact Waste 27(3). https://doi.org/10.1061/JHTRBP.HZENG-1187

Osinubi KJ, Amadi AA (2010) Evaluation of hydraulic conductivity of compacted iron ore tailings–bentonite mixtures. J ASTM Int 7(5):1–12

Osinubi KJ, Nwaiwu CMO (2006) Design of compacted lateritic soil liners and covers. J Geotech Geoenviron Eng 132(2):203–213. https://doi.org/10.1061/(ASCE)1090-0241(2006)132:2(203)

Osinubi KJ, Eberemu AO, Amadi AA (2015) Pozzolanic stabilization of tailings and tropical soils for barrier applications. Waste Manag 38:202–211

Osinubi KJ, Yohanna P, Eberemu AO (2019) Blast furnace slag re-utilization in geotechnical containment barriers: a review. Environ Earth Sci 78(14):412

Owolabi TA, Daramola SO (2024) Geotechnical properties and applications of iron ore tailings amended lateritic soil for road construction. Rud Geol Naft Zb 41(1):157–170

Raviteja KV, Janga JK, Reddy KR (2024) Hydraulic conductivity of bentonite amended flyash liners for MSW landfills. In: Geotechnical engineering challenges to meet current and emerging needs of society. CRC Press, pp 3265–3269. https://doi.org/10.1201/9781003431749-643

Samani N et al (2020) Stabilization of iron ore tailings with cement and bentonite: a case study on Golgohar mine. Bull Eng Geol Environ. https://doi.org/10.1007/s10064-020-01843-6

Seed HB, Chan CK (1959) Structure and strength characteristics of compacted clays. J Soil Mech Found Div 85(5):87–128. https://doi.org/10.1061/JSFEAQ.0000229

Vanapalli SK, Fredlund DG, Pufahl DE (1999) The influence of soil structure and stress history on the soil-water characteristics of a compacted till. Géotechnique 49(2):143–159. https://doi.org/10.1680/geot.1999.49.2.143

van Genuchten MT (1980) A closed-form equation for predicting the hydraulic conductivity of unsaturated soils. Soil Sci Soc Am J 44(5):892–898. https://doi.org/10.2136/sssaj1980.03615995004400050002x

Vitor OA, Laura S, Philippe JPG, Ana PK, Ivo AHS (2023) Application of leached iron ore tailings to produce sustainable cements. Constr Build Mater 377:131095. https://doi.org/10.1016/j.conbuildmat.2023.131095

Wu W, Kang K, Ye Q, Luo A, Zhang J, Wang J, Shi S (2026) Comprehensive utilization of iron ore tailings: a review of sustainable practices and technologies. Min Metall Explor 1–18

Wu X, Yang F, Huang S (2024) Predicting CBR values using Gaussian process regression and meta-heuristic algorithms in geotechnical engineering. Multiscale Multidiscip Model Exp Des 7(4):3799–3813

Zhang W, Li H, Phoon KK (2022) Application of Gaussian process regression in geotechnical property prediction and uncertainty quantification. Comput Geotech 141:104499. https://doi.org/10.1016/j.compgeo.2021.104499